Serveur Académique Lausannois SERVAL serval.unil.ch

Author Manuscript
Faculty of Biology and Medicine Publication

This paper has been peer-reviewed but does not include the final publisher proof-corrections or journal pagination.

Published in final edited form as:

serval
serveur académique lausannois

UNIL | Université de Lausanne
Faculté de biologie
et de médecine

Loss of mesenchymal *CSL* signaling leads to field cancerization and multifocal epithelial tumors

Bing Hu[1], **Einar Castillo**[1], **Louise Harewood**[2], **Paola Ostano**[3], **Alexandre Reymond**[2], **Reinhard Dummer**[4], **Wassim Raffoul**[5], **Wolfram Hoetzenecker**[6,7], **Günther F. L. Hofbauer**[4], and **G. Paolo Dotto**[1,7,*]

[1]Department of Biochemistry, University of Lausanne, Epalinges, CH-1066, Switzerland; [2]Center for Integrative Genomics (CIG), University of Lausanne, Lausanne, CH-1015, Switzerland; [3]Cancer Genomics Laboratory, Edo and Elvo Tempia Valenta Foundation, Biella, 13900, Italy; [4]Department of Dermatology, University Hospital Zurich, Zurich, CH-8091, Switzerland; [5]Department of Plastic, Reconstructive and Aesthetic Surgery, University Hospital of Lausanne, Lausanne, CH-1011, Switzerland; [6]Department of Dermatology, University of Tübingen, Tübingen, D-72076, Germany; [7]Cutaneous Biology Research Center, Massachusetts General Hospital, Charlestown, MA 02129, USA.

Summary

It is currently unclear whether tissue changes surrounding multifocal epithelial tumors are a cause or consequence of cancer. Here, we provide evidence that loss of mesenchymal *Notch/CSL* signaling causes tissue alterations, including stromal atrophy and inflammation, which precede and are potent triggers for epithelial tumors. Mice carrying a mesenchymal-specific deletion of *CSL/RBP-Jκ*, a key *Notch* effector, exhibit spontaneous multifocal keratinocyte tumors that develop after dermal atrophy and inflammation. *CSL*-deficient dermal fibroblasts promote increased tumor cell proliferation through up-regulation of *c-Jun* and *c-Fos* expression and consequently higher levels of diffusible growth factors, inflammatory cytokines, and matrix remodeling enzymes. In human skin samples, stromal fields adjacent to cutaneous squamous cell carcinomas and multifocal premalignant actinic keratosis lesions exhibit decreased *Notch/CSL* signaling and associated molecular changes. Importantly, these changes in gene expression are also induced by UVA, a known environmental cause of cutaneous field cancerization and skin cancer.

Keywords

epithelial-mesenchymal interactions; epithelial cancer; Cancer Associated Fibroblasts; *in situ* carcinoma; actinic keratosis; *Notch*; AP-1

*Corresponding author: Paolo.Dotto@unil.ch.

Introduction

Squamous cell carcinomas are very common malignant tumors in humans, occurring in organs such as skin, oral mucosa and upper digestive tract, lung, and urogenital apparatus. Analysis of these tumors led, more than 60 years ago, to the concept of field cancerization, based on the frequent tumor multiplicity and associated changes of both epithelial and mesenchymal tissues beyond the neoplastic area (Slaughter et al., 1953). Genetic and epigenetic changes of the epithelium have been implicated as likely primary determinants of the field cancerization process (Chai and Brown, 2009), while alterations of the underlying mesenchyme have received relatively little attention. The reasons for stromal alterations, including widespread atrophic changes (Slaughter et al., 1953), are also not understood.

Notch signaling is a form of cell-cell communication with a key role in development and tissue homeostasis (Artavanis-Tsakonas et al., 1999). The mammalian *Notch* gene family codes for four closely related transmembrane receptors, whose activation depends on similar mechanisms of ligand binding, proteolytic cleavage and nuclear translocation (Kopan and Ilagan, 2009). The activated Notch intracellular domain associates with the DNA binding protein CSL (CBF-1 in human and RBP-Jκ in mouse) converting it from a repressor into an activator of transcription (Kopan and Ilagan, 2009). While *Notch*-independent functions of *CSL* have also been reported, loss of function experiments have indicated that, in most mammalian systems, *CSL* functions mainly as a *Notch* effector (Kopan and Ilagan, 2009).

The biological function of *Notch/CSL* is highly context dependent. In the skin, this pathway plays a well-established function in keratinocyte differentiation and tumor suppression, through both intracellular and paracrine growth control mechanisms (Demehri et al., 2009; Dotto, 2008; Restivo et al., 2011; Watt et al., 2008; Williams et al., 2011). By contrast, the role of this pathway in the mesenchymal compartment of the skin has been explored to a very limited extent. We show here that mesenchymal loss of the *CSL/RBP-Jκ* gene is sufficient to induce in the skin several features associated with field cancerization, which are amenable to increased AP1 levels and activity. These findings are of likely clinical significance, as suppression of *Notch/CSL* signaling and associated gene expression events occur in stromal fields adjacent to cutaneous premalignant actinic keratosis lesions, and can be induced by UVA exposure, a major cause of skin chronic and cancer-predisposing alterations.

Results

1) Spontaneous multifocal keratinocyte tumors in mice with mesenchymal *CSL/RBP-Jk* deletion

We recently reported that maintenance of the hair follicle keratinocyte cell fate is compromised in mice with mesenchymal deletion of the *CSL/RBP-Jk* gene (*Col*ICre x *RBP-Jκ* loxP/loxP), due to intrinsically defective dermal papilla cells (Hu et al., 2010). These same mice, by 2-4 months after birth, spontaneously developed multiple keratinocyte tumors histologically resembling squamous cell carcinoma (SCC) precursor lesions of the actinic keratosis / Bowen's disease type (Fig. 1A-D; Fig. S1A). These lesions were characterized by irregular architecture/expansion of the epidermis, acanthosis, dyskeratosis and several features of incipient malignant disease, including discontinued laminin basement membrane deposition, co-expression of epithelial and mesenchymal markers, and microinvasion (Fig. 1A,B, and data not shown). Tumor stroma alterations included expression of cancer-associated fibroblast (CAF) markers (S100A4, alpha Smooth Muscle Actin) and cancer associated matrix proteins (Tenascin C, Periostin) with a gradient of expression (Fig. S1A, D). Increased matrix metalloprotease levels and inflammatory infiltrates were also observed (data not shown). In 6 months old mice, tumors exhibited features of malignant SCCs, with

aberrant keratinization, pronounced dysplasia and inflammatory infiltration, and invasion of epithelial islands or spindle-shaped cells into dermis and connective tissue (Fig. 1E, F; Fig. S1B,C). Tumors could be successfully transplanted (data not shown).

DNA analysis of dissociated tumor cells separated from surrounding stroma showed no deletion of the *RBP-Jκ* gene nor mutations in the *p53* and the *Ha-*, *Ki-* and *N-ras* genes (Fig.S1D,E and data not shown). Comparative genomic hybridization (CGH) revealed small chromosomal aberrations in all examined tumors (Fig. 1G and Table S1A). Chromosomal alterations in tumors from the same mice were only partially overlapping, pointing to multifocal origin or separate clonal evolution, while specific chromosomal regions were similarly affected in tumors from different mice (Fig 1G, Table S1A). These regions and/or their human equivalents have been implicated in cancer development, most frequently epithelial, like murine 7qC (human 15q11.2) and 8qA1.3 (Table S2). qPCR confirmed alterations of these regions in the CGH analyzed tumors and/or tumors from additional mice (Fig. 1H, Table S1B).

For insights into gene expression, we used laser capture microdissection (LCM) of spontaneously occurring tumors in parallel with normal epidermis from the same mice. Expression of *ATF3*, an AP1-related transcription factor with a positive role in keratinocyte tumorigenesis (Wu et al., 2010), was increased in all LCM-dissected tumors (Fig. 1I), while growth inhibitory genes like *TGF-ß* family members, $p15^{Ink4b}$, $p16^{Ink4a}$, $p21^{WAF1/Cip1}$ and *Notch1* were down-modulated (Fig. 1J). Among positive growth regulatory genes, *c-Myc, cyclin D1, CDK4, CDK6, E2F1, p63-* and *Wnt*-related genes were not up-regulated or even decreased and, consistent with the complex role of *NF-κB* signaling in keratinocytes (Hinata et al., 2003), members of this family were differentially modulated (Fig. S1F).

2) Early skin changes in mice with mesenchymal *CSL/RBP-Jκ* deletion

Stromal atrophy was linked with field cancerization in the initial clinical report (Slaughter et al., 1953). Decreased dermal thickness and reduced elastic fibers and collagen content were found in skin of mutant mice at birth, when hair follicle are still normal (Hu et al., 2010) (Fig. 2A-C; Fig. S2A,B), and at 3 weeks of age, in regions of conserved hair follicle structure and density and when both mutant and control mice had entered the telogen phase of the hair cycle (Fig. 2A, Fig. S2A,C). Collagen I and Elastin mRNA expression was unaffected (not shown), while Collagen I protein levels were reduced in skin of mutant mice, with increased ratio of soluble versus insoluble forms (Fig. 2D). Consistent with a proteolytic mechanism, mutant mice had elevated dermal MMP activity already at birth (Fig. 2E). Expression of a CAF marker, Periostin, but not Tenascin C, was also increased in these mice at this time (Fig. S2D and data not shown). Dermal fibroblasts density and proliferative index were similar to controls, with lower apoptosis (Fig. S2E-G).

BrdU labeling indicated that proliferation of interfollicular keratinocytes was already increased in P0 mutant mice (Fig. 2F). This was accompanied by increase of phosphorylated activated form of Fibroblast Growth Factor Receptor 1, which occurred already in mutant E16.5-E18.5 embryos (Fig. 2G,H) together with augmented expression of mitogenic FGFs by underlying dermal fibroblasts (shown below). Loricrin, a differentiation marker important for skin barrier function, was down-modulated in mutant E16.5-E18.5 embryos and P0 mice (Fig. 2I), with increased transepidermal water loss (TEWL) at birth that normalized in later days (Fig. S2H).

LCM, followed by qRT-PCR, showed loss of RBP-Jκ expression in mutant embryos dermis, with no decrease in epidermis (Fig. S2I). Parallel qRT-PCR analysis confirmed decreased loricrin expression in epidermis of mutant embryos and P0 mice, with similar down-modulation of another late differentiation marker, *SPRR1a* (Fig. 2J). RT-PCR analysis

showed also deregulation of many growth factors and cytokines in epidermis of mutant embryos and mice, which may contribute to their later phenotype (Fig. 2J).

3) Role of inflammation in spontaneous skin tumor development

Inflammation is an important determinant of chronic tissue alterations leading to cancer. Inflammatory cells, identified by anti-CD45 staining, became detectable in dermis of mutant mice a few days after birth, followed by localized inflammatory infiltrates and concomitant expression of Tenascin C and, in overlying epidermis, Keratin 6, a marker of epidermal hyperplasia (Fig. 2K). Foci of inflammatory infiltrates and Tenascin C and Keratin 6 expression expanded significantly in subsequent days (Fig. 2K), together with recruitment of macrophages (Fig. 2K,L). LCM of stromal tissue followed by qPCR showed similar levels of *RBP-Jκ* gene deletion in unaffected versus focally altered areas (Fig. S2L), pointing to the importance of more indirect events.

For wider view of skin than permitted by immunohistochemical analysis, we adopted a technique, Fluorescence Diagnosis (FD), used in the clinic for imaging of hyperplastic, premalignant and malignant keratinocytic lesions (Krammer and Plaetzer, 2008). FD is based on preferential uptake of 5-aminolevulinic acid (5-ALA) by hyperproliferative cells and conversion into porphyrins detectable by fluorescence excitation. Relative to littermate controls, back skin of mutant mice already exhibited stronger and widespread FD signal at birth (Fig. 3A), consistent with increased keratinocyte proliferation detected by BrdU labeling (Fig. 2F). Discrete regions of higher FD positivity, likely corresponding to foci of inflammatory infiltration and epidermal hyperplasia, were also found, which increased in number over time, eventually coalescing and marking areas of multifocal tumor development (Fig. 3A,B).

To assess the role of inflammation, (*ColI*-Cre x *RBP-Jκ*^loxP/loxP^) mice were treated with Celebrex, a broad anti-inflammatory agent and COX-2 inhibitor. When treatment was started at birth, strength and expansion of FD signal, as well as eventual tumor formation, were significantly counteracted, even if not totally suppressed (Fig. 3C,D; Fig. S3A). By contrast, no such effects were observed when the treatment was initiated after tumor development (Fig. S3B), consistent with the chromosomal alterations that have occurred by this time and findings that suppression of inflammation can prevent but not reverse tumorigenesis (Colotta et al., 2009).

4) Tumor enhancing mechanisms of *CSL*-deficient dermal fibroblasts

Full-thickness grafting of skin of mice with the mesenchymal *CSL/RBP-Jκ* deletion onto immuno-compromised animals resulted in similar epidermal hyperproliferation and underlying dermal alterations, such as increased Tenascin C and MMP3 expression and decreased elastic fibers and collagen content. With time, the grafts gave rise to tumors similar to those of the original mice (data not shown).

To assess whether dermal fibroblasts with *CSL/RBP-Jκ* deletion were intrinsically endowed with tumor-promoting capability, they were admixed with weakly tumorigenic mouse (Pam212) (Roop et al., 1983) or human (SCC13) (Rheinwald and Beckett, 1981) keratinocyte lines, followed by injection into immune compromised mice at the dermal-epidermal junction, i.e. a location approximating that of malignant skin tumor formation (Wu et al., 2010). Tumors formed in the presence of *RBP-Jκ* −/− fibroblasts were significantly larger than controls (Fig. 4A), with increased proliferation (Fig. 4B) and cellularity (Fig. 4C) and decreased differentiation (Fig. 4D). There was disruption of Laminin basement membrane deposition (Fig. 4E), loss of E-Cadherin (Fig. 4F) and increased MMP3 production in surrounding matrix (Fig. 4G).

An important question was whether fibroblasts with *RBP-Jκ* deficiency can also impact on normal keratinocytes prior to transformation. Intra-dermal injection of human primary keratinocytes (HKCs) in combination with control fibroblasts gave rise to large epidermal islands with tightly adherent layers of keratinocytes and pronounced granular layer differentiation (Fig. 4H). By contrast, HKCs admixed with *RBP-Jκ* −/− fibroblasts gave rise to islands with loosely connected keratinocytes and signs of cellular atypia (Fig. 4H), higher BrdU labeling index (Fig. 4I) and decreased expression of "early" differentiation markers like Keratin 1 (Fig. 4J). Basement membrane laminin deposition was uneven (Fig. 4K), with increased Tenascin C and Periostin expression in surrounding stroma (Fig. 4L,M).

To probe into underlying mechanisms, freshly isolated fibroblasts from P0 mice with and without *RBP-Jκ* deletion were analyzed for expression of growth factors/cytokines, matrix components and remodeling enzymes. Growth factor genes such as *FGF7* and *10*, *Igf2*, and *CSF-1*, which promote keratinocyte proliferation and/or inflammation (Wagner et al., 2010; Werner et al., 2007), were up-regulated in several independent preparations of *RBP-Jκ* −/− fibroblasts versus controls (Fig. S4A). Matrix metallo-proteases (*MMP2*, *3*, *9* and *13*) and *Tenascin C* and *Periostin* were similarly up-regulated (Fig. S4A). Expression of *alpha Smooth Muscle Actin* (*ACTA2*) and *PDFG Receptor α isoform* (*PDGFRα*) was also enhanced, while that of other CAF markers, like *PDGFRβ*, *FAP*, *S100A4* and *Desmin*, was not affected or even decreased (Fig. S4A and data not shown). Similar modulation of gene expression was observed with cultured dermal fibroblasts from *RBPJk* −/− mice and fibroblasts with the "floxed" *RBP-Jκ* gene after "acute" deletion by a Cre-expressing adenovirus (Fig. S4B,C). Dermal fibroblasts express both Notch 1 and 2 receptors. siRNA-mediated knockdown of *Notch1* and, to a greater extent, *Notch2* resulted in suppression of the canonical *Hes1* target gene and concomitant up-regulation of genes induced by the *RBP-Jk* deletion (Fig. S4D).

For further insights, we resorted to cDNA microarray analysis of dermal fibroblasts from P0 mice plus/minus *RBP-Jκ* deletion in parallel with cultured dermal fibroblasts plus/minus deletion of the "floxed" *RBP-Jκ* gene by Ad-Cre. 381 genes were found similarly modulated as a consequence of *RBP-Jκ* deletion. Among significant biological processes to which up-regulated genes could be assigned were "DNA damage and Stress Response", "tissue remodeling and wound repair", "vasodilation" and "inflammatory response" (Fig. S4E). c-Jun/AP1 was a prominent transcription factor in the network that could be built from the validated set of genes deregulated by *RBP-Jκ* deletion (Fig. S4F). Involvement of various AP1 family members was assessed further below. Other relevant genes included mediators of cell-matrix and cell–cell interactions (*CD44*, *Syndecan-1* (*SDC1*), Hyaluronan synthase 2 (*HAS2*) and Hyaluronan-mediated motility receptor (*HMMR*), kinases (*MAP2K3*, *MAPK6*, *MAPK14*, *Prkar2a*) and trascription factors (*Ets1* and *NFATc3*) involved in stress and/or growth responses, and determinants of inflammation (*COX2*, *CSF-1*, *IL17RA*). Increased expression of these genes, as well as of *FGF7* and *FGF10*, was confirmed by LCM and qRT-PCR of dermis from P0 mutant versus wild type mice, and E16.5 and E18.5 embryos (Fig. S4G).

Mesenchymal loss of the *PTEN* gene was reported to enhance mammary tumor development driven by transgenic oncogene expression, with induction of a CAF phenotype that overlaps only partially with the one caused by *RBP-Jκ* deletion (Trimboli et al., 2009). Given previous work linking Notch signaling to control of *PTEN* expression (Demarest et al., 2008), we examined expression of this gene, but found similar levels in mutant fibroblasts and controls (Fig. S4A,B).

A common feature of many genes up-regulated in *RBP-Jκ* −/− fibroblasts is that they are under positive AP-1 control. *Notch/RBP-Jκ* signaling can function as negative regulator of

AP-1 activity, also through modulation of various AP-1 family members (Chu et al., 2002; Talora et al., 2002). Consistent with these previous findings, expression of several AP1 family members was up-regulated in dermal fibroblasts from mutant mice and embryos (Fig. 5A-C; Fig. S4G; Fig. S5A,B), and fibroblasts with *Notch1* and *Notch2* knock-down (Fig. S4D).

To assess which AP1 family members are more functionally important, we evaluated the consequences of their knocked down expression in *RBP-Jκ* –/–fibroblasts. Down-modulation of *c-Jun* or *c-Fos* returned expression of all tested growth factors, cytokines, matrix components and MMPs to levels close to control cells (Fig. 5D, Fig. S5C,D). Knockdown of other AP1 family members could counteract up-regulation of *MMP3* expression, while had more limited and selective effects on other genes (Fig. S5E).

To assess the *in vivo* significance of these findings, *RBP-Jκ* –/– fibroblasts transfected with anti-c-Jun siRNAs versus scrambled controls were admixed with SCC13 cells, followed by intradermal injection into mice. Tumors formed in the presence of *RBP-Jκ* –/– fibroblasts with c-Jun knockdown had lower weight, with pronounced apoptosis/necrosis of cells in central areas and reduced proliferation, and enhanced differentiation of cells at the periphery (Fig. 5E-H, Fig. S5F-I). Differences in tumor formation were accompanied by decreased expression of CAF markers in surrounding stroma together with decreased MMP expression and activity (Fig. 5I, J; and data not shown).

5) Relevance to human skin

An important question was whether down-modulation of CSL signaling can lead to a CAF-like phenotype in human cells. shRNA-mediated knock-down of *CSL* (*RBP-Jκ*) in 2 independent strains of human primary dermal fibroblasts resulted in reduced expression of the "canonical" *Notch* targets *Hes1* and *Hes5*, as well as of *Notch1* and *2* receptors, and *Notch* ligands *Jagged 1* and 2 (Fig. 6A; Fig. S6). Expression of *c-Jun* and *c-Fos*, and many other genes up-regulated in mouse *RBP-Jk* –/– cells, was similarly affected in human dermal fibroblasts with *CSL* knockdown (Fig. 6A; Fig. S6A,B). As in xenografts with mouse fibroblasts, SCC13 cells admixed with human dermal fibroblasts with *CSL* knockdown formed tumors of greater size and cellularity and more disordered differentiation than the controls, with up-regulation of Tenascin C and Periostin expression in surrounding stroma (Fig. 6B-D; Fig. S6C and data not shown).

To assess the relevance of the above findings to the clinical situation, we used LCM of surgically excised skin samples from patients with lesions preceding SCC formation. Analysis of stroma underlying areas of premalignant lesions (actinic keratosis, AK) along with skin fields farther away, revealed consistent inverse relation between expression of *Notch* receptors, *Hes1* and *Hes5* versus *c-Jun*, *c-Fos* and other genes under negative *Notch/ CSL* control, like, CAF markers, *CD44* and *COX-2*, in the lesion-underlying stroma (Fig. 7A). The LCM and qRT-PCR results were further validated by immunofluorescence analysis of excised skin regions, showing decreased Notch2 signal intensity with concomitant up-regulation of c-Jun in the Vimentin-positive cells of the AK-underlying stroma versus flanking skin (Fig. 7B; Fig. S7A-C).

UV light exposure is a major etio-pathological agent of premalignant and malignant skin cancer formation (Rittie and Fisher, 2002). While UVB has limited penetration power and its effects are mostly limited to epidermal cells, UVA can also directly affect cells of underlying dermis. UVA - but not UVB - irradiation of human skin explants followed by LCM of upper dermal compartment and qRT-PCR showed significant down-modulation of *Notch1*, *Notch2* and *Hes1* genes even at lowest doses, while *c-Jun* expression was up-regulated (Fig. 7C and data not shown). In time course experiments, modulation of these

genes occurred as early as 1 hour after UVA exposure and persisted up to 5 days (Fig. 7C; Fig. S7D-F).

For further insights, we focused on the *Notch2* gene. As with skin explants, down-modulation of this gene, and up-regulation of *c-Jun*, occurred in cultured human dermal fibroblasts, within 20′ of UVA exposure, persisting up to 5 days (Fig. S7G). Nascent *Notch2* transcripts, detected by qRT-PCR of the first exon-intron junction, were also down-regulated at late times of UVA exposure as mature transcripts (Fig. S7G). Persistent down-modulation would be consistent with a permanent modification of the *Notch2* transcription locus. In fact, PCR analysis of methylation-enriched DNA samples from dermal compartment of skin explants and cultured dermal fibroblasts, indicated that the GC-rich region of the *Notch2* promoter was increasingly methylated as a function of time after UVA exposure, with no increased methylation of a distal GC-rich region of the same gene (Fig. 7D and Fig. S7H). Importantly, similar differences in methylation of the *Notch2* promoter were found in the clinical situation, in stroma underlying AK lesions versus skin fields further away (Fig. 7E).

Discussion

Field cancerization is a clinical condition of major significance for cancer recurrence and lethality, which is still poorly understood (Chai and Brown, 2009). It can develop at various body sites, among which the skin is the most common. Development of mouse genetic models to probe into underlying molecular defects would be highly desirable. The skin phenotype of mice with mesenchymal RBP-Jκ deletion presents several features that are reminiscent of those found in field cancerization. The clinical process is associated with a "diagnostic triad" of multifocal tumors, expanding alterations of the surrounding epithelium and atrophic changes of the underlying stroma (Slaughter et al., 1953). Among these, the stromal atrophy of *RBP-Jκ* mutant mice is a feature that has not yet been observed, to our knowledge, in any other mouse cancer model. The similarity to the clinical situation of expanding multifocal lesions detected by the fluorescence diagnosis technique is also remarkable.

The earliest biochemical alterations resulting from *RBP-Jκ* deletion in dermal fibroblasts include increased expression of genes with mitogenic and/or pro-inflammatory function in both fibroblasts and overlying keratinocytes. These in turn can elicit further changes, most notably an inflammatory reaction, both directly and through transiently compromised skin barrier function. Recruitment of inflammatory cells is followed by localized infiltrates, possibly by an initially weak (and stochastic) signal, which is then amplified by an immunological cascade. Locally increased inflammation is likely to be a determining factor of other focal changes in dermis and overlying epidermal tissue. Inflammation is also known to increase chromosomal instability (Colotta et al., 2009) and could thus contribute to later multifocal tumors, which we found associated with specific chromosomal alterations. Treatment of *RBPJκ* mutant mice with a COX-2 inhibitor as anti-inflammatory agent delayed formation of focal lesions and tumors, raising the exciting prospect that, even in patients with field cancerization, inhibition of inflammation, even if not sufficient to reverse tumorigenesis, could be used to prevent or retard secondary tumor development. In line with this possibility is our other finding that COX-2 expression is up-regulated in both mouse and human fibroblasts by loss of *CSL/RBP-Jκ* function and in the clinical situation, in stroma underlying actinic keratosis lesions versus skin fields further away.

Similar changes in gene expression were elicited by loss or down-modulation of the *CSL* gene and knock-down of *Notch1* and *Notch2*. These included up-regulated expression of several AP1 family members. Consistent with their shared key role (Eferl and Wagner,

2003), down-modulation of *c-Jun* or *c-Fos* had the most significant effects in *RBP-Jκ* deficient fibroblasts, reverting expression of all tested deregulated genes. Even *in vivo*, the tumor enhancing effects of RBP-Jκ −/− fibroblasts were counteracted by the *c-Jun* knockdown. Importantly, an inverse relationship between *Notch/CSL* activity and *c-Jun/c-Fos* expression was also found in excised skin samples from enrolled patients with cutaneous field cancerization, in stromal fields underlying actinic keratosis versus distant normal epidermis.

Basal level of *Notch* activity in dermal cells (as also observed by use of a reporter mouse, our unpublished observations) can be explained by concomitant expression of Notch receptors and ligands by the same or neighboring cells. In the present context, we were concerned with exogenous signals that cause down-regulation of this pathway. Cutaneous field cancerization usually develops in sun-exposed areas in elderly people or immunosuppressed patients, and is defined by the appearance of multiple actinic keratosis lesions on damaged skin. UVA light exposure can directly affect the dermis and its importance in UV-induced carcinogenesis is increasingly recognized (Ridley et al., 2009). We have found that UVA, but not UVB, exposure has a rapid negative impact on expression of Notch receptors and downstream targets in the dermis of human skin explants and dermal fibroblasts, in parallel with *c-Jun* and *c-Fos* up-regulation. This is in contrast to the consequences of UVB exposure of human epidermis and keratinocytes, which elicits a *p53*-dependent upregulation of *Notch1* expression as a pro-survival and pro-differentiation reaction (Mandinova et al., 2008; Yugawa et al., 2007).

A very early consequence of UVA exposure is production of radical oxygen species (ROS) with consequent ligand-independent activation of EGFR/ERK/AP1 signaling (Rittie and Fisher, 2002). While increased ERK/AP1 activity can negatively regulate *Notch1* expression and activity (Kolev et al., 2008), down-modulation of *Notch* signaling enhances AP1 activity. Thus, a negative feedback loop between the two pathways can be involved in the initial impact of UVA exposure on gene expression. A concomitant attractive mechanism is provided by epigenetic modifications, which we have found to occur shortly after UVA exposure at level of the *Notch2* promoter. This is consistent with recent findings of a recruitment of DNA methyltransferase I (DNMT1) and methylation of selective GC rich promoters in rapid response to increased ROS levels (O'Hagan et al., 2011). DNA methylation of the *Notch2* promoter could account for sustained down-modulation of the gene and be of considerable clinical significance, as we found that the *Notch2* promoter is also differentially methylated *in vivo*, in actinic keratosis underlying stroma versus skin fields further away. DNA methyl transferase inhibitors are already approved for clinical trials of cancer treatment (Baylin and Jones, 2011) and an exciting possibility is that these compounds can also be employed for preventing and/or reversing stromal alterations associated with field cancerization.

Methods

Mice and human samples

Development of mice with mesenchymal *RBP-Jκ* deletion was previously reported (Hu et al., 2010) . All mouse work was performed according to the Swiss guidelines and regulations for the care and use of laboratory animals. Human skin samples for primary cell preparation were obtained from abdominoplasty procedures at the Department of Plastic, Reconstructive and Aesthetic Surgery, Lausanne University Hospital (Switzerland) with patients' and institutional approvals. Samples of actinic keratosis and SCC were obtained from clinical biopsies at the Departments of Dermatology, University of Tübingen (Germany), and Zurich University Hospital (Switzerland). Parts not needed for histological diagnosis were further processed with institutional review board approval.

Cell and tissue manipulations

Conditions for culturing of cells, organ explants, viral infection and siRNA transfection were previously reported (Hu et al., 2010; Kolev et al., 2008; Wu et al., 2010). Full thickness grafting of mouse skin (Hu et al., 2010) and intradermal tumorigenicity assays (Wu et al., 2010) were also as described. Detailed conditions for cell culture and *in vivo* testing are provided in the web supplementary information. UV exposure was performed in a Bio-Link crosslinker UV irradiation system (Vilber Lourmat) equipped with exchangeable UVA (375nm) and UVB (312nm) lamps. The exposure dosage was measured with a portable photometer IL1400A (International Light Technologies).

For more details and skin organ culture, collagen determination, LCM, and anti-inflammatory treatment please see *Extended Experimental Procedures*. The list of siRNAs and shRNAs used for this study is provided in Table S3.

qRT-PCR and cDNA microarray analysis, LCM and methylated DNA detection

Conditions for qRT-PCR, immunoblotting and immunofluorescence and cDNA microarray analysis were as previously described (Hu et al., 2010; Nguyen et al., 2006). The list of gene-specific primers is provided in Table S3. PCR arrays were from SAbiosciences (PAMM-041). LCM was performed using an Arcturus XT microdissection system (Applied Biosystems), as before (Hu et al., 2010). Methylated DNA was isolated using MethylCollector (Active Motif) according to the manufacturer's protocol. Recovered DNA was quantified with a Nanodrop 1000 spectrophotometer (Nanodrop) prior to qPCR analysis.

Immunodetection

Antibodies are listed in Table S3. Immunofluorescence images were acquired with a Zeiss LSM510 meta laser-scanning microscope. For quantitation of Notch 2 immunofluorescence signal, digitally acquired images for each color channel were separately imported into Image J software and converted into binary images. The numbers of pixels (representing the intensity of the fluorescence signal) were measured using "Measurement" function. For single cell Notch2 signaling measurement, Vimentin positive single cells were selected using "Lasso Tool" in Photoshop Element 8.0 software (Adobe) and the Notch2 signal were read out by histogram and calculated in Microsoft Excel 2004 software (Microsoft).

Fluorescence diagnosis

Newborn or adult mice (with back skin shaved 24 hours before treatment) were topically applied 5-ALA mix (containing 10% ALA w/w (Sigma) and 20% DMSO, diluted in distilled water) at a dosage of $10mg/cm^2$. 3 hours later, mice were analyzed under a Xenogen IVIS-200 optical *in vivo* imaging system (Caliper Life Sciences) with excitation wavelength at 430nm and emission wavelength at 640nm, using a DSRed filter at 1.5 cm depth and 10 second exposure time (f2). The binning setting was 2 pixels per bin and field of View (FOV) was 24. Intensity of the emitted signal was calculated using Living Image 3.2 software (Caliper Life Sciences). For newborn animals (P0-P6), the minimum/maximum of reading was set at 3.5e6/8e7 photons/s; for adult mice the minimum/maximum was set at 3e7/3e8.

Array Comparative Genomic Hybridization (CGH)

Excised skin tumors were minced into small pieces and digested in 1% Collagenase I (Sigma; 37°C for 1 hour) for removal of stromal tissue. The resulting suspension was filtered through a 40mm mesh and epithelial fragments were used for DNA extraction, using a Wizard® Genomic DNA Purification Kit (Promega). Tumor DNA samples were labelled

with Cy3 and hybridized to Nimblegen mouse CGH arrays together with Cy5-labelled normal brain DNA extracted from the same mice. Arrays contained 2.1 million probes across the whole genome based on the MM9 genome build. CGH was according to Nimblegen protocols. Scanning with an Agilent G2565BA Microarray Scanner was followed by image and data processing using Nimblescan software v.2.5. Data can be accessed through the Gene Expression Omnibus number: pending.

Statistical analysis

PRISM software (Graph Pad Software Inc.) was used to assess statistical significance of the results, employing one-way ANOVA followed by Bonferroni's test, except for RNAi experiments for *Jun B*, *Jun D*, *FosB*, *FosL1*, *FoL2*, and shRNA experiments, where Dunnett's test was applied.

Supplementary Material

Refer to Web version on PubMed Central for supplementary material.

Acknowledgments

References

Artavanis-Tsakonas S, Rand MD, Lake RJ. Notch signaling: cell fate control and signal integration in development. Science. 1999; 284:770–776. [PubMed: 10221902]

Baylin SB, Jones PA. A decade of exploring the cancer epigenome -biological and translational implications. Nat Rev Cancer. 2011; 11:726–734. [PubMed: 21941284]

Chai H, Brown RE. Field effect in cancer-an update. Ann Clin Lab Sci. 2009; 39:331–337. [PubMed: 19880759]

Chu J, Jeffries S, Norton JE, Capobianco AJ, Bresnick EH. Repression of activator protein-1-mediated transcriptional activation by the Notch-1 intracellular domain. J Biol Chem. 2002; 277:7587–7597. [PubMed: 11739397]

Colotta F, Allavena P, Sica A, Garlanda C, Mantovani A. Cancer-related inflammation, the seventh hallmark of cancer: links to genetic instability. Carcinogenesis. 2009; 30:1073–1081. [PubMed: 19468060]

Demarest RM, Ratti F, Capobianco AJ. It's T-ALL about Notch. Oncogene. 2008; 27:5082–5091. [PubMed: 18758476]

Demehri S, Turkoz A, Kopan R. Epidermal Notch1 loss promotes skin tumorigenesis by impacting the stromal microenvironment. Cancer Cell. 2009; 16:55–66. [PubMed: 19573812]

Dotto GP. Notch tumor suppressor function. Oncogene. 2008; 27:5115–5123. [PubMed: 18758480]

Eferl R, Wagner EF. AP-1: a double-edged sword in tumorigenesis. Nat Rev Cancer. 2003; 3:859–868. [PubMed: 14668816]

Hinata K, Gervin AM, Zhang Y. Jennifer, Khavari PA. Divergent gene regulation and growth effects by NF-kappa B in epithelial and mesenchymal cells of human skin. Oncogene. 2003; 22:1955–1964. [PubMed: 12673201]

Hu B, Lefort K, Qiu W, Nguyen BC, Rajaram RD, Castillo E, He F, Chen Y, Angel P, Brisken C, et al. Control of hair follicle cell fate by underlying mesenchyme through a CSL-Wnt5a-FoxN1 regulatory axis. Genes Dev. 2010; 24:1519–1532. [PubMed: 20634318]

Kolev V, Mandinova A, Guinea-Viniegra J, Hu B, Lefort K, Lambertini C, Neel V, Dummer R, Wagner EF, Dotto GP. EGFR signalling as a negative regulator of Notch1 gene transcription and function in proliferating keratinocytes and cancer. Nat Cell Biol. 2008; 10:902–911. [PubMed: 18604200]

Kopan R, Ilagan MX. The canonical Notch signaling pathway: unfolding the activation mechanism. Cell. 2009; 137:216–233. [PubMed: 19379690]

Krammer B, Plaetzer K. ALA and its clinical impact, from bench to bedside. Photochem Photobiol Sci. 2008; 7:283–289. [PubMed: 18389144]

Mandinova A, Lefort K, di Vignano A. Tommasi, Stonely W, Ostano P, Chiorino G, Iwaki H, Nakanishi J, Dotto GP. The FoxO3a gene is a key negative target of canonical Notch signalling in the keratinocyte UVB response. Embo J. 2008; 27:1243–1254. [PubMed: 18388864]

Nguyen BC, Lefort K, Mandinova A, Antonini D, Devgan V, Della Gatta G, Koster MI, Zhang Z, Wang J, di Vignano AT, et al. Cross-regulation between Notch and p63 in keratinocyte commitment to differentiation. Genes Dev. 2006; 20:1028–1042. [PubMed: 16618808]

O'Hagan HM, Wang W, Sen S, Destefano Shields C, Lee SS, Zhang YW, Clements EG, Cai Y, Van Neste L, Easwaran H, et al. Oxidative damage targets complexes containing DNA methyltransferases, SIRT1, and polycomb members to promoter CpG Islands. Cancer Cell. 2011; 20:606–619. [PubMed: 22094255]

Restivo G, Nguyen B-C, Dziunycz P, Ristorcelli E, Ryan J, Ozuyal Y, Di Piazza M, Radtke F, Dixon M, Hofbauer G, et al. IRF6 is a mediator of Notch pro-differentiation and tumour suppressive function in keratinocytes. EMBO J. 2011 in press.

Rheinwald JG, Beckett MA. Tumorigenic keratinocyte lines requiring anchorage and fibroblast support cultures from human squamous cell carcinomas. Cancer Res. 1981; 41:1657–1663. [PubMed: 7214336]

Ridley AJ, Whiteside JR, McMillan TJ, Allinson SL. Cellular and sub-cellular responses to UVA in relation to carcinogenesis. Int J Radiat Biol. 2009; 85:177–195. [PubMed: 19296341]

Rittie L, Fisher GJ. UV-light-induced signal cascades and skin aging. Ageing Res Rev. 2002; 1:705–720. [PubMed: 12208239]

Roop DR, Hawley-Nelson P, Cheng CK, Yuspa SH. Expression of keratin genes in mouse epidermis and normal and malignantly transformed epidermal cells in culture. J Invest Dermatol. 1983; 81:144s–149s. [PubMed: 6190960]

Slaughter DP, Southwick HW, Smejkal W. Field cancerization in oral stratified squamous epithelium; clinical implications of multicentric origin. Cancer. 1953; 6:963–968. [PubMed: 13094644]

Talora C, Sgroi DC, Crum CP, Dotto GP. Specific down-modulation of Notch1 signaling in cervical cancer cells is required for sustained HPV-E6/E7 expression and late steps of malignant transformation. Genes Dev. 2002; 16:2252–2263. [PubMed: 12208848]

Trimboli AJ, Cantemir-Stone CZ, Li F, Wallace JA, Merchant A, Creasap N, Thompson JC, Caserta E, Wang H, Chong JL, et al. Pten in stromal fibroblasts suppresses mammary epithelial tumours. Nature. 2009; 461:1084–1091. [PubMed: 19847259]

Troy T, Jekic-McMullen D, Sambucetti L, Rice B. Quantitative comparison of the sensitivity of detection of fluorescent and bioluminescent reporters in animal models. Mol Imaging. 2004; 3:9–23. [PubMed: 15142408]

Wagner EF, Schonthaler HB, Guinea-Viniegra J, Tschachler E. Psoriasis: what we have learned from mouse models. Nat Rev Rheumatol. 2010

Watt FM, Estrach S, Ambler CA. Epidermal Notch signalling: differentiation, cancer and adhesion. Curr Opin Cell Biol. 2008; 20:171–179. [PubMed: 18342499]

Werner S, Krieg T, Smola H. Keratinocyte-fibroblast interactions in wound healing. J Invest Dermatol. 2007; 127:998–1008. [PubMed: 17435785]

Williams SE, Beronja S, Pasolli HA, Fuchs E. Asymmetric cell divisions promote Notch-dependent epidermal differentiation. Nature. 2011; 470:353–358. [PubMed: 21331036]

Wu X, Nguyen BC, Dziunycz P, Chang S, Brooks Y, Lefort K, Hofbauer GF, Dotto GP. Opposing roles for calcineurin and ATF3 in squamous skin cancer. Nature. 2010; 465:368–372. [PubMed: 20485437]

Yugawa T, Handa K, Narisawa-Saito M, Ohno S, Fujita M, Kiyono T. Regulation of Notch1 gene expression by p53 in epithelial cells. Mol Cell Biol. 2007; 27:3732–3742. [PubMed: 17353266]

Highlights

1. Mesenchymal loss of *CSL/Notch* results in field cancerization of the skin

2. Pro-tumorigenic consequences of CSL loss are linked to *c-Jun/c-Fos* upregulation

3. Anti-inflammatory treatment counteracts the field cancerization phenotype

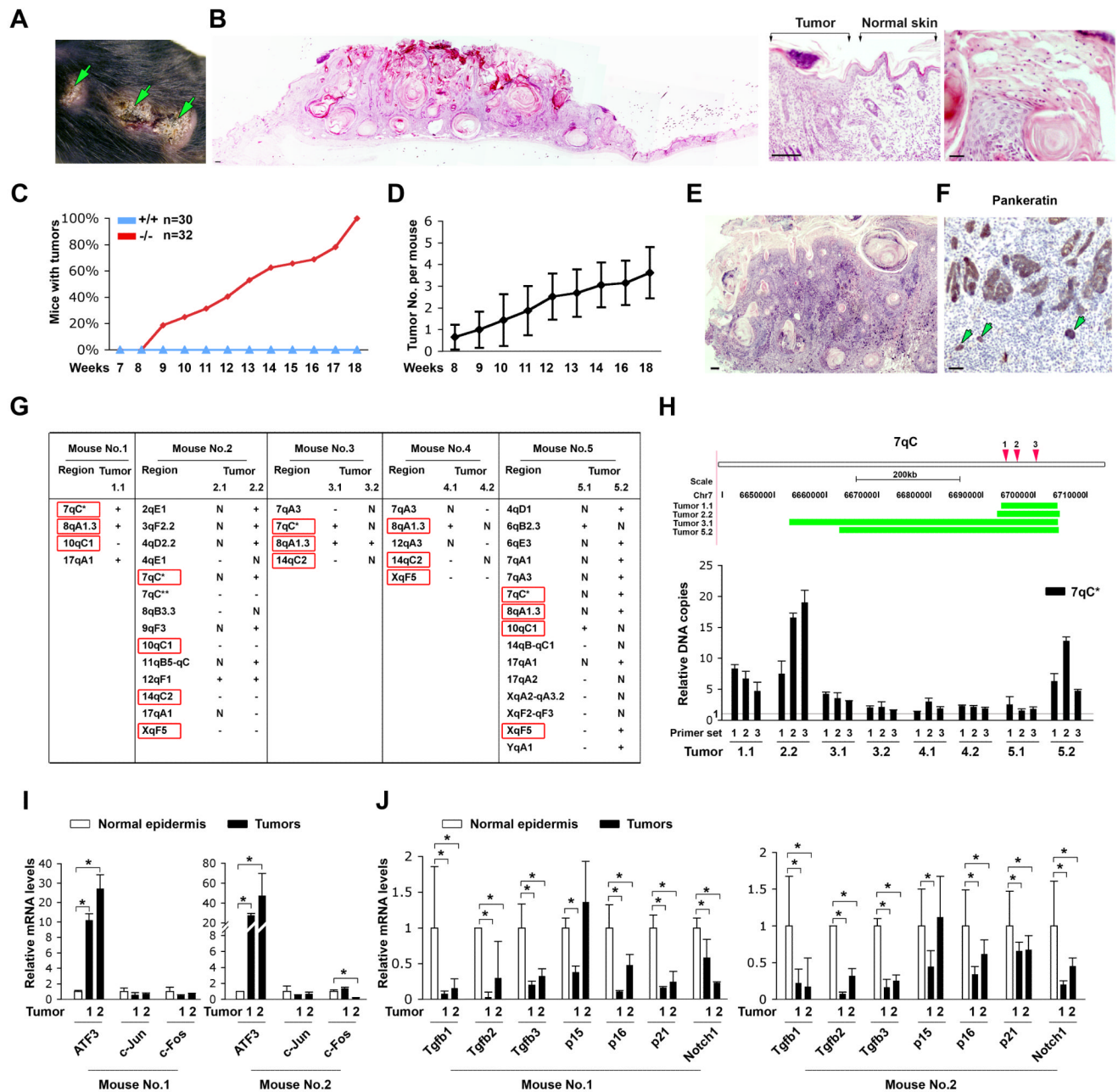4. UVA exposure down-modulates Notch signaling and expression through DNA methylation

Figure 1. Mesenchymal *CSL/RBP-Jκ* deletion results in spontaneous skin tumor formation

(A) Overview of multiple spontaneous skin tumors in a mouse with mesenchymal *RBP-Jκ* deletion (*ColI*-Cre x *RBP-Jκ*$^{loxP/loxP}$) at 4 months.

(B) Low and high magnification histological images of spontaneous tumors and surrounding skin in 4 months old mice. Tumors at this stage exhibited features of *in situ* carcinomas of keratoacanthoma and/or Bowen's disease type, with disrupted epidermal architecture, parakeratotic nuclei and foci of aberrant keratinization. Immunohistochemical analysis of tumor stromal component is shown in Fig. S1A, D.

(C) Number of tumor-bearing mice with mesenchymal *RBP-Jk* deletion (–/–) versus littermate controls (+/+) until 18 weeks after birth or earlier, if mice had to be sacrificed due

to tumor burden. Fraction of males and females was similar, with no differences in tumor formation.

(D) Number of independent (physically separated) tumors in mutant mice. Shown are average tumor numbers per mouse per time point, as well as variation among individual mice. Values may be underestimated, due to coalescence of individual lesions.

(E) Histology of skin tumors in mice at 6 months of age. Higher magnification analysis showed loss of epidermal architecture, pronounced cellular atypia and inflammatory infiltration (Fig. S1B). Lesions with similar characteristics were found in 7 of 7 mice that survived until this age. Tumors were classified as well to moderately differentiated SCCs (Grade I-II).

(F) Immunohistochemical analysis with anti-Pankeratin antibodies showing invading epithelial islands and tumor front in a 6 months old mouse. Quantification of results is provided in Fig. S1C.

(G) Summary of CGH DNA analysis of skin tumors versus unrelated normal tissue (brain) from the same mice. For each tumors are listed specific chromosomal regions that were duplicated (+), deleted (−) or, for pairs of tumors derived from the same mouse, unaffected (N). Raw CGH data and statistical significance are provided in Table S1A. Statistical permutation tests showed that the repeated identification of 4 overlapping rearrangements in 5 mice (as found, for instance, for 7qC and 8qA) is highly significant (P = 0.0005).

(H) Upper : Map of mouse chromosomal 7qC region and overlapping segments of duplication (green bars) in the indicated multiple tumors. Maps of other chromosomal regions with overlapping alterations in multiple tumors are provided in Table S1A. Lower: qPCR analysis of tumor and normal DNA samples utilized for CGH was performed with primers for three sites within the 7qC region (indicated by arrows in the previous panel). Results are in arbitrary units after internal normalization for an unrelated chromosomal region (15qB3.1). Similar results were obtained after normalization for three other chromosomal regions (5qC1 and 13qB1, data not shown). Further qPCR analysis showed duplications of the 7qC and 8qA regions in 4 and 5 additional tumors, respectively, out of 6 that were analyzed, from 3 more mice (Table S1B).

(I) and (J), qRT-PCR analysis of LCM samples from tumors versus flanking normal epidermis (identified by double immunofluorescence with anti-K14 and -Tenascin C antibodies, as shown in Fig. S1D) from two mice, two tumors per mouse. Expression of indicated genes is in arbitrary units utilizing *ß-Actin* for normalization. Analysis of other genes is in Fig. S1F. *: p<0.01 by one way ANOVA followed by Bonferroni's test. Scale bars: 200μm for B and D; 40μm for C and E.
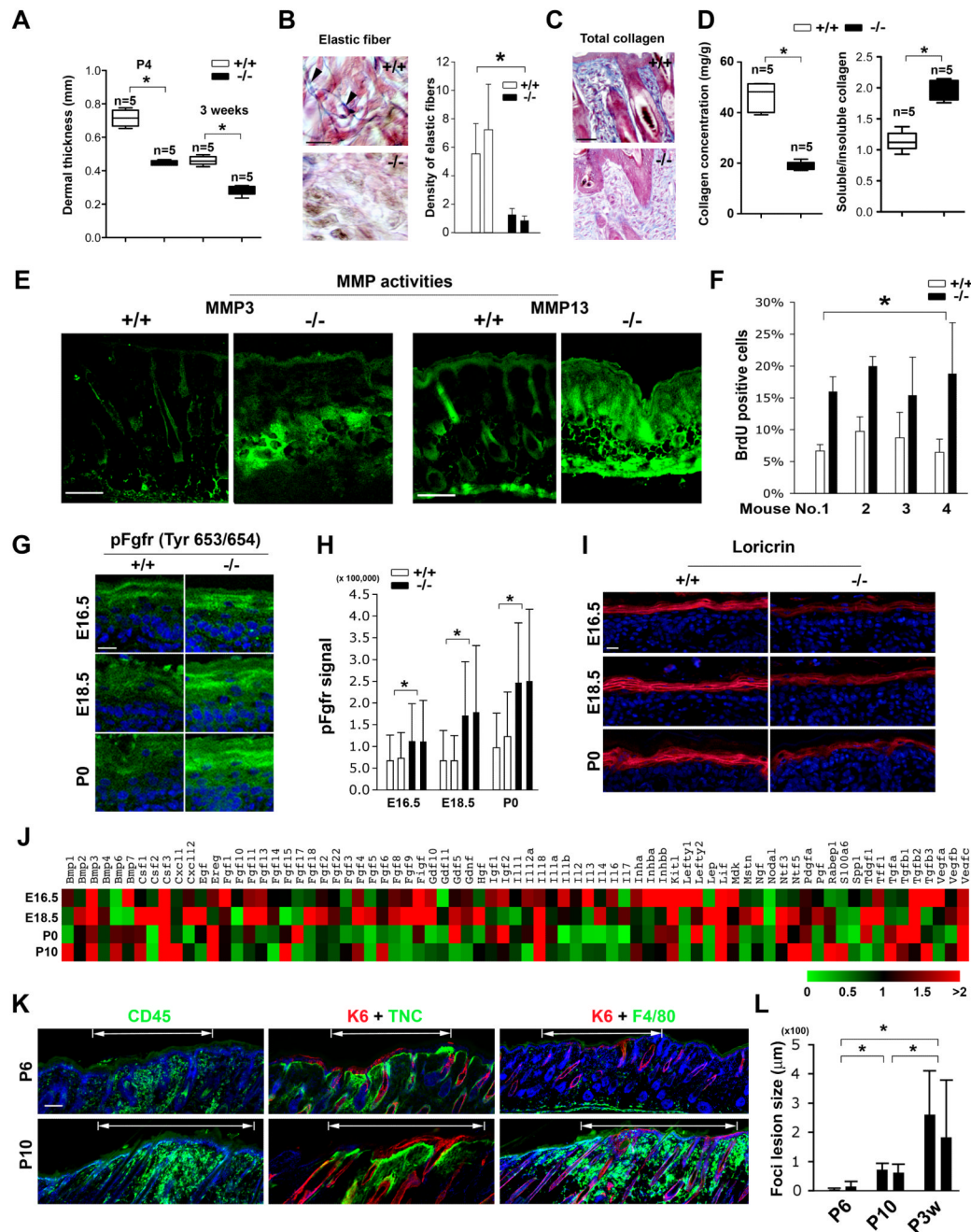
Figure. 2. Early skin defects in mice with mesenchymal *CSL/RBP-Jκ* deletion

(A) Dermal thickness (distance between dermal-epidermal junction and panniculum carnosum; double end arrows) was quantified in five *RBP-Jκ* mutant mice and five controls (black and white bars) at 4 days and 3 weeks of age (* p<0.01). Histological images are in Fig. S2A.

(B) Verhoeff-Masson-trichrome staining and quantification of elastic fibers (x10^5/mm^2) in back skin dermis of two P4 mice per genotype, counting 3 independent fields for each section (* p<0.01).

(C) Masson-trichrome staining of total collagen in P4 mouse skin (blue) with Nuclear Fast Red for counterstaining. Images are representative of four mice per genotype. Collagen I and III immunostaining is in Fig. S2B.

(D) Biochemical quantification of total collagen and ratio of soluble versus insoluble fractions in 3 weeks old mice. 5 mice per genotype were analyzed. (* p<0.01).

(E) *In situ* zymography of P4 mouse skin with MMP3 and MMP13 preferential substrates. Little signal was observed in presence of MMP inhibitor GM6001 (not shown). MMP activity in epidermis and hair follicles is likely due to diffusion, consistent with *MMP3* and *MMP13* mRNA levels being increased selectively in fibroblast compartment of *RBP-Jκ* mutant mice (Fig. S4A and data not shown). Increased MMP3 and MMP13 protein expression in skin of mutant mice was also observed by immunohistochemistry (not shown).

(F) P0 mice were injected with BrdU, followed by BrdU labeling determination in interfollicular epidermis. Four mice per genotype were analyzed (* p<0.01).

(G) Immunofluorescence of back skin sections of E16.5 and E18.5 embryos and P0 mice with antibodies recognizing the activated phospho-Tyr 653/654 form of FGFR1 and, to a less extent, other FGF receptors. Images are representative of 3-4 independent fields, 2 mice per genotype.

(H) Immunofluorescence signal intensity in epidermal compartment of above skin samples by computer-assisted quantification (* < 0.01).

(I) Immunofluorescence of back skin sections of E16.5 and E18.5 embryos and P0 mice with antibodies against Loricrin. Images are representative of 3-4 independent fields, 2 mice per genotype.

(J) Epidermal compartment of E16.5 and E18.5 embryos and P0 mice was analyzed by LCM followed and RT-PCR arrays for cytokines and growth factors. Results are shown as heat map fold changes of expression of indicated genes in mutant versus control samples.

(K) Immunofluorescence analysis of P6 and P10 mouse back skin, illustrating foci of leukocyte infiltration (CD45 positive) and Keratin 6 (K6) and Tenascin C expression. Parallel immunofluorescence with anti-K6 and F4/80 antibodies illustrated hyperplastic epithelium and infiltrating macrophages, respectively.

(L) Quantification of focal lesion size (CD45 positive areas demarked by arrows in the previous panel) showing a time-dependent increase. Large skin sections, 5 lesions per mouse, two mice per time point, were analyzed (*<0.01).

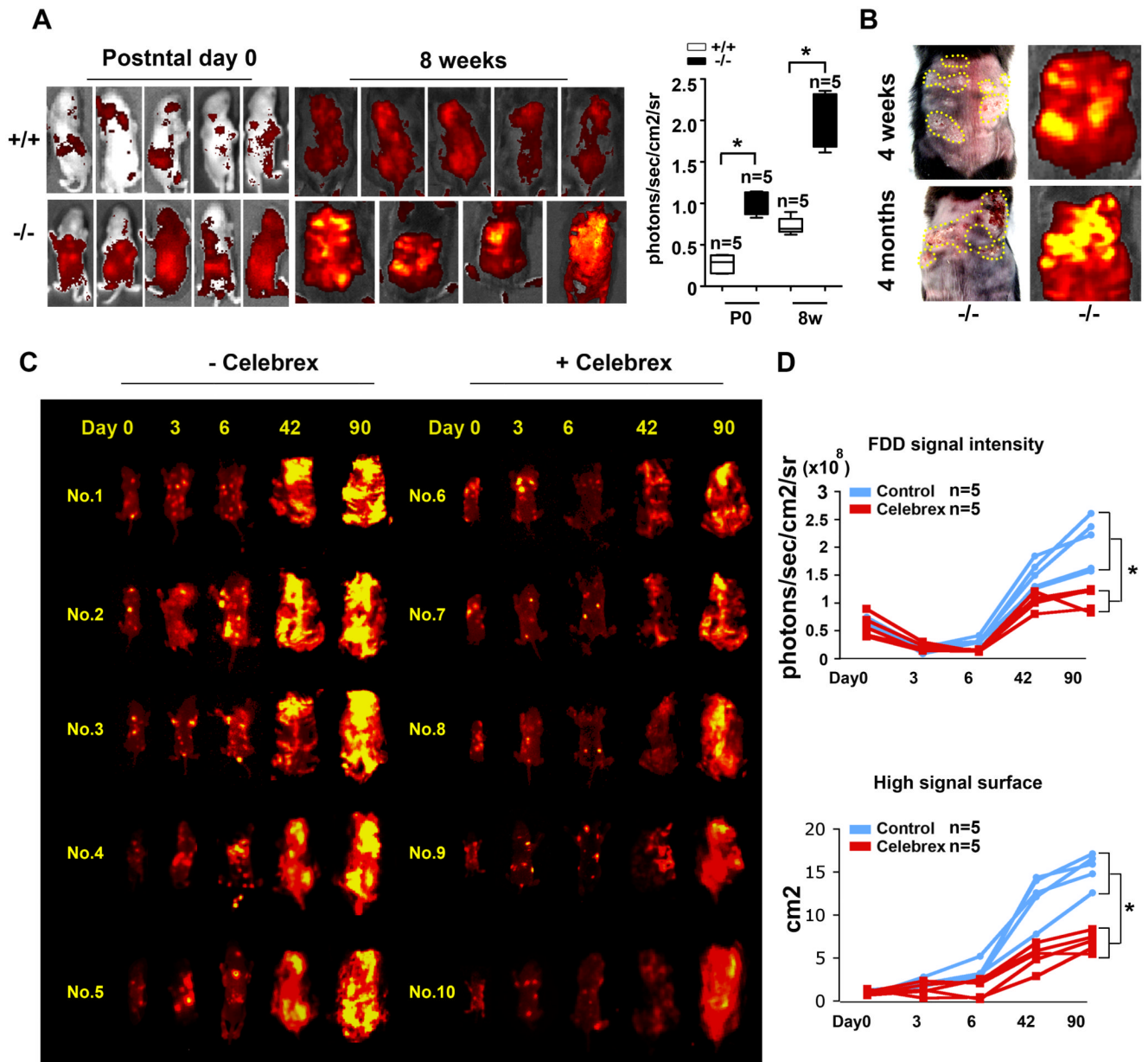Scale bars: 20μm for A, C, G and I; 200 μm for E and K.

Figure 3. Expanding multifocal skin lesions and counteracting effects of anti-inflammatory treatment as detected by Fluorescence Diagnosis (FD)

(A) Mice at indicated times after birth were topically treated with 5-ALA, followed by fluorescent light excitation and digital image acquisition, using same exposure conditions for age-matched mutant (−/−) and control (+/+) animals. FD signal intensity (x1e8 photons/sec/cm^2/sr) was calculated as in (Troy et al., 2004) (* $p<0.01$).

(B) Intense FD positivity in mouse mutant back skin at > 4 weeks of age corresponds to multifocal areas of tumor development (areas of macroscopic pictures marked by dotted lines).

(C) Mice with mesenchymal *RBP-Jκ* deletion were treated, starting at birth, with the COX2 inhibitor Celebrex or vehicle alone (intraperitoneal injections, 20μg per g body weight, in DMSO, twice weekly, 5 mice per group), followed by FD analysis at indicated times.

(D) Quantification of FD signal intensity and body surface with high FD signal (above a threshold of 2e7 photons/sec/cm^2/sr for mice up to 6 days old and 1.5e8 photons/sec/cm^2/sr for older mice) for each mouse (*<0.01). For macroscopic and histological images of mice at the end of the experiment, see Fig. S3A.
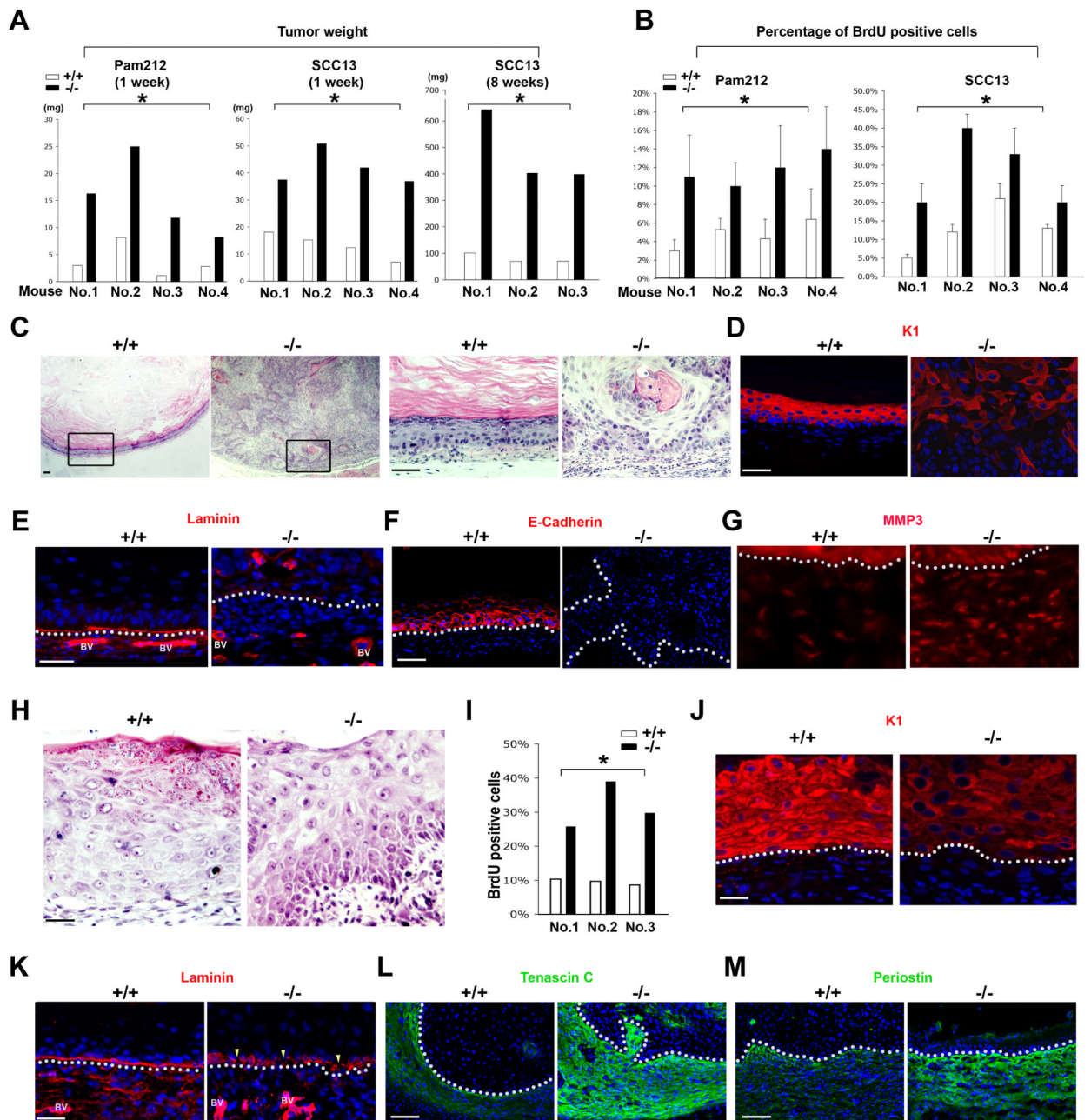
Figure 4. *RBP-Jκ* deficient dermal fibroblasts enhance growth/tumorigenic behavior of SCC-derived and normal primary keratinocytes

(A) Weakly tumorigenic mouse (Pam212) or human (SCC13) keratinocytes were admixed with cultured (second passage) dermal fibroblasts from mice plus/minus *RBP-Jκ* deletion prior to injection at the dermal-epidermal junction of NMRI athymic mice. Mice were sacrificed for tumour weight determination either 1 or 8 weeks later. Weight difference between tumor pairs in each mouse and between the two groups of tumors was highly significant (* p<0.01).

(B) Mice as in previous panel were BrdU labeled for 2 hours prior to sacrifice, followed by determination of BrdU labeling of keratinocyte tumor cells (identified by Keratin 14 staining) in presence of control versus *RBP-Jκ* –/– fibroblasts (* p<0.01).

(C) Histological analysis of tumors formed by SCC13 cells admixed with dermal fibroblasts plus/minus *RBP-Jκ* deletion 8 weeks after injection. Shown are low and corresponding high magnification images (left and right panels, boxed areas).

(D-G) Immunofluorescence analysis of the indicated proteins in tumors formed by SCC13 cells admixed with fibroblasts plus/minus *RBP-Jκ* deletion. Besides the epithelial-mesenchymal border, basement membrane of underlying blood vessels (BV) is also positive for Laminin staining (E). Dotted lines mark the epithelial-mesenchymal junction. Nuclei were visualized by DAPI staining.

(H) Histological images of epidermal islands formed by HKCs admixed with control versus *RBP-Jκ* −/− fibroblasts 1 week after intra-dermal mouse injection. Note granular layer differentiation features in epidermal islands formed in presence of control but not mutant fibroblasts.

(I) Mice as in previous panel were BrdU labeled for 2 hours prior to sacrifice, followed by determination of BrdU labeling of keratinocytes (identified by Keratin 14 staining) in the presence of control versus mutant fibroblasts (* $p<0.01$).

(J-M) Immunofluorescence analysis of epidermal islands formed by HKCs together with control versus mutant fibroblasts with antibodies against indicated proteins. Scale bars: 40μm for C-F, L and M; 20μm for G, H, J and K.
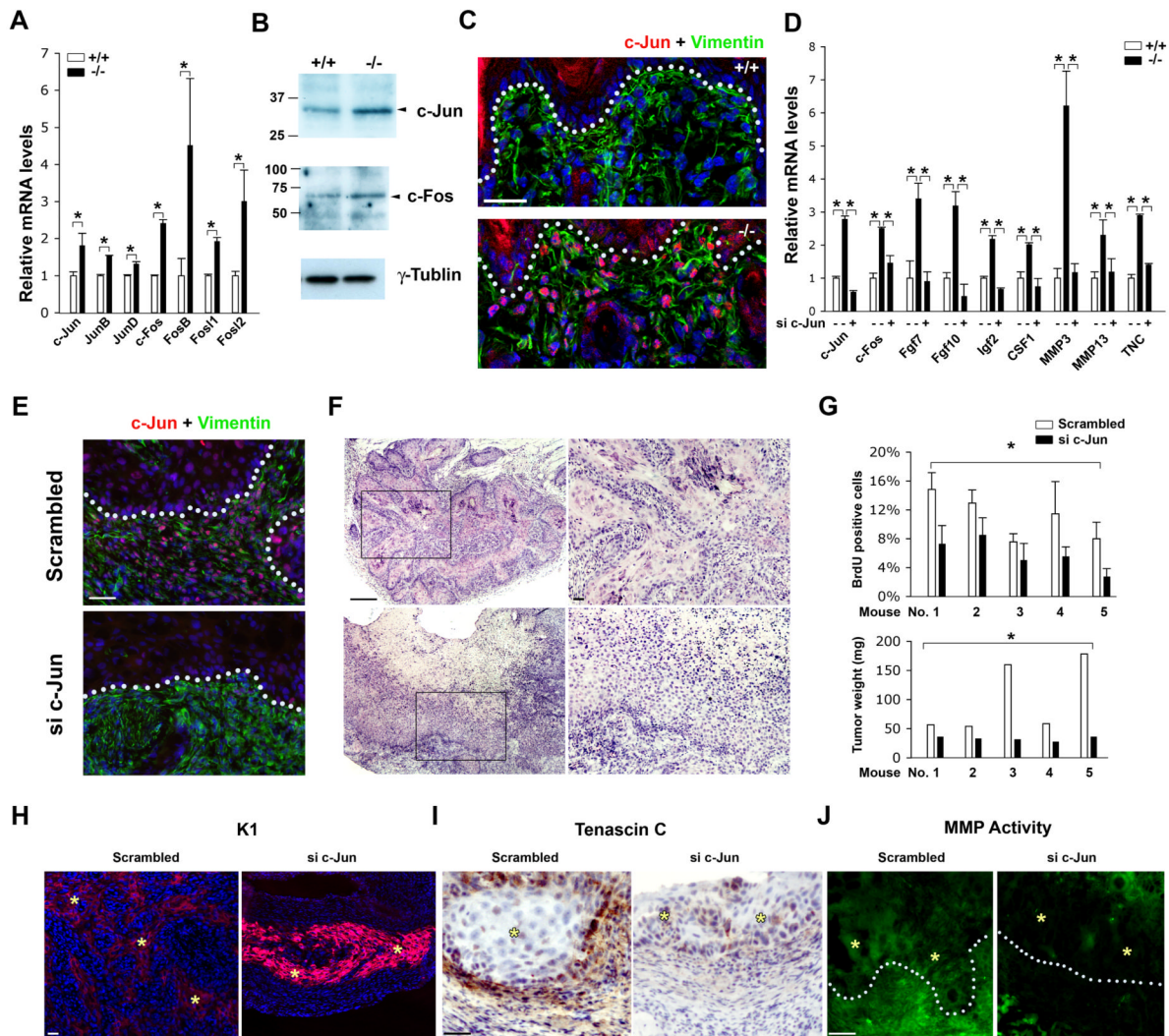
Figure 5. Dermal *RBP-Jκ* regulates tumor growth through AP-1

(A) Differential expression of AP-1 family members in dermal fibroblasts freshly isolated from a pool of three newborn mice (P0) plus/minus *RBP-Jκ* deletion. qRTPCR results are in arbitrary values after normalization for *β-Actin* (* p<0.01).

(B) Immunoblot analysis of c-Jun and c-Fos expression in freshly isolated dermal fibroblasts from P0 mice. Densitometric scanning of autoradiographs with normalization for γ-Tubulin showed, respectively, a 2 and 1.5 fold increase of c-Jun and c-Fos expression in mutant versus control cells.

(C) Immunofluorescence analysis of c-Jun (red) expression in back skin of P0 mice. Dermal fibroblasts were identified by co-staining with anti-Vimentin (green) antibodies. Dotted lines mark dermal-epidermal borders. Additional immunofluorescence images with antibodies against c-Jun and phospho-c-Jun and results quantification are provided in Fig. S5A,B.

(D) Expression of indicated genes in dermal fibroblasts with *RBP-Jκ* deletion plus/minus siRNA-mediated *c-Jun* knockdown, in parallel with similarly cultured control fibroblasts (black and white bars, respectively). qRT-PCR results are expressed in arbitrary units with *β-Actin* for normalization (* p<0.01). Similar results with a second set of siRNA against *c-Jun*, and siRNAs against *c-Fos* are shown in Fig. S5C,D. Functional consequences of knock-down of other AP1 family members are shown in Fig. S5E.

(E) Immunofluorescence analysis of c-Jun expression in tumors formed 1 week after intradermal injection of SCC13 cells admixed with *RBP-Jκ* deficient dermal fibroblasts transfected with siRNA against *c-Jun* or scrambled siRNA control. Dermal fibroblasts were identified by co-staining with anti-Vimentin antibodies. Tumor-stromal border is indicated by dotted lines. Similar results were obtained by immunofluorescence analysis of the other tumors formed in presence of dermal fibroblasts plus/minus *c-Jun* knock-down, and are consistent with biochemical analysis of cultured cells, showing persistent knockdown effects for at least one week after siRNA transfection.

(F) Histological analysis of tumors formed by SCC13 cells admixed with *RBP-Jκ* deficient fibroblasts plus/minus *c-Jun* knock-down as in the previous panel. To minimize individual animal variations, mice were injected in parallel with the two combinations of cells. Shown are low and corresponding high magnification images (left and right panels, boxed areas). In the tumor formed by SCC13 cells admixed with *RBP-Jκ* −/− fibroblasts with c-Jun knock-down, pronounced apoptosis and necrosis of cells in the more central areas resulted in tissue loss - and an empty space -at the time of cutting. Similar findings were obtained with other 4 tumor pairs as shown in Fig. S5F-I, and with 5 additional tumor pairs from an independent experiment (not shown).

(G) Mice as in (E,F) were BrdU labeled for 2 hrs prior to sacrifice. BrdU labeling of tumor keratinocytes (identified by Keratin 14 staining) admixed with *RBP-Jκ* deficient fibroblasts plus/minus *c-Jun* knockdown (black and white bars, respectively) was determined in parallel with tumor weight (* $p<0.01$).

(H-J) Same samples were analyzed by immunostaining for Keratin 1 (H) and Tenascin C (I) and *in situ* zymography with a preferential MMP13 substrate (J). Asterisks indicate the epithelial tumor compartment.

Scale bars: 20μm for C, E, F (right two panels), H-J; 200μm for F (left two panels).
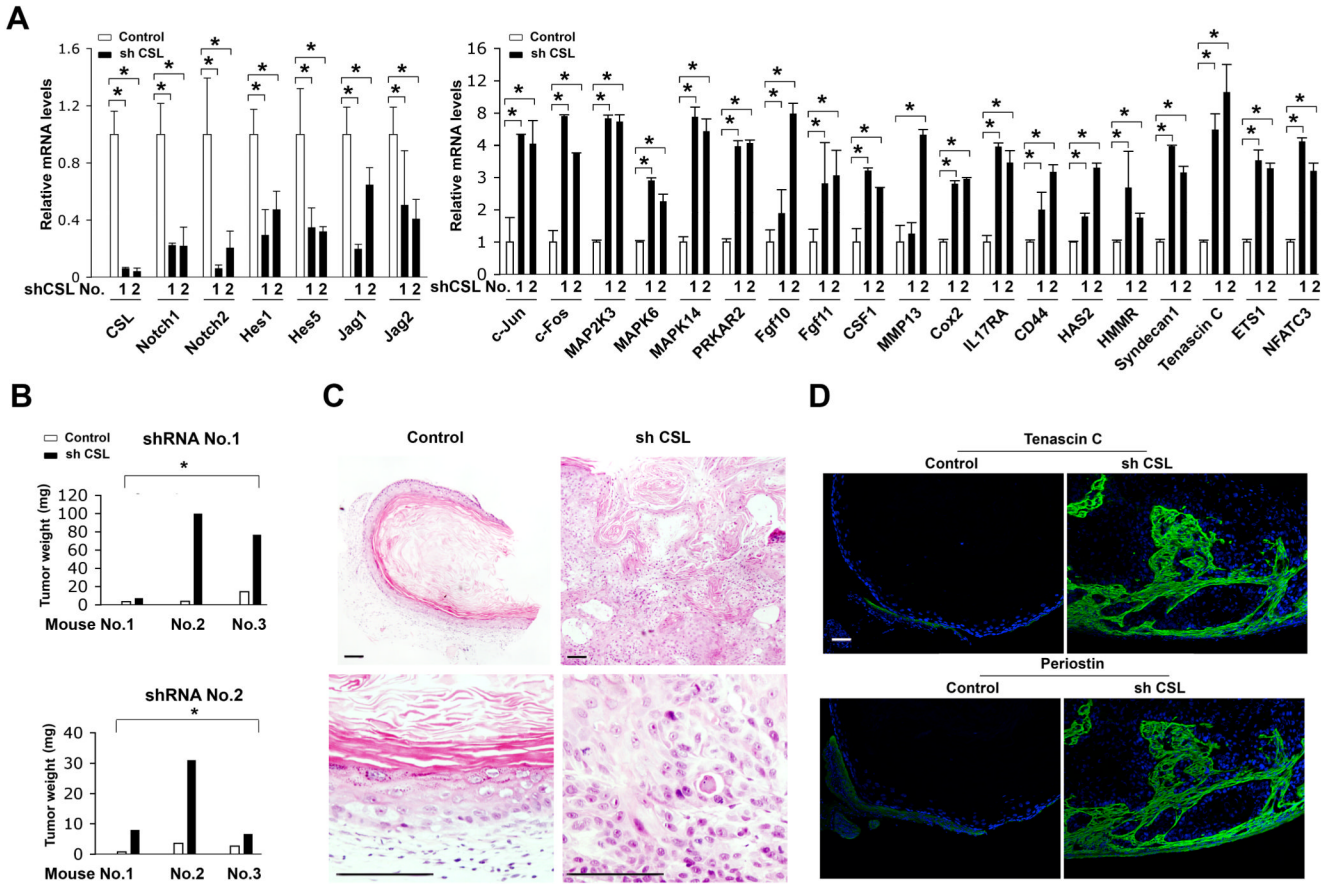
Figure 6. Tumor-enhancing phenotype of human dermal fibroblasts with *CSL* knock-down

(A) Human dermal fibroblasts (HDFs) were infected with two anti-CSL shRNA lentiviral vectors (#1 and 2; black bars) in parallel with empty vector control (white bar), followed by 6 days selection for puromycin resistance. Cells were analyzed by qRT-PCR for indicated genes, using *36β4* for normalization(*p<0.01). Analysis of an independent strain of HDFs plus/minus *CSL* knockdown is shown in Fig. S6A,B.

(B) SCC13 keratinocytes were admixed with HDFs plus/minus *CSL* knockdown (by shRNA vector #1) prior to intra-dermal injection into NMRI athymic mice. Each mouse received parallel injections of keratinocytes admixed with control versus *CSL* knockdown fibroblasts (white and black bars, respectively). Mice were sacrificed for tumor weight determination 8 weeks later (* p<0.01).

(C) Histological analysis of tumors formed by SCC13 cells admixed with HDFs plus/minus *CSL* knockdown. Shown are low and high magnification images. Histological analysis of other tumors is shown in Fig. S6C.

(D) Immunofluorescence analysis of tumors from the above experiment with antibodies against indicated proteins.
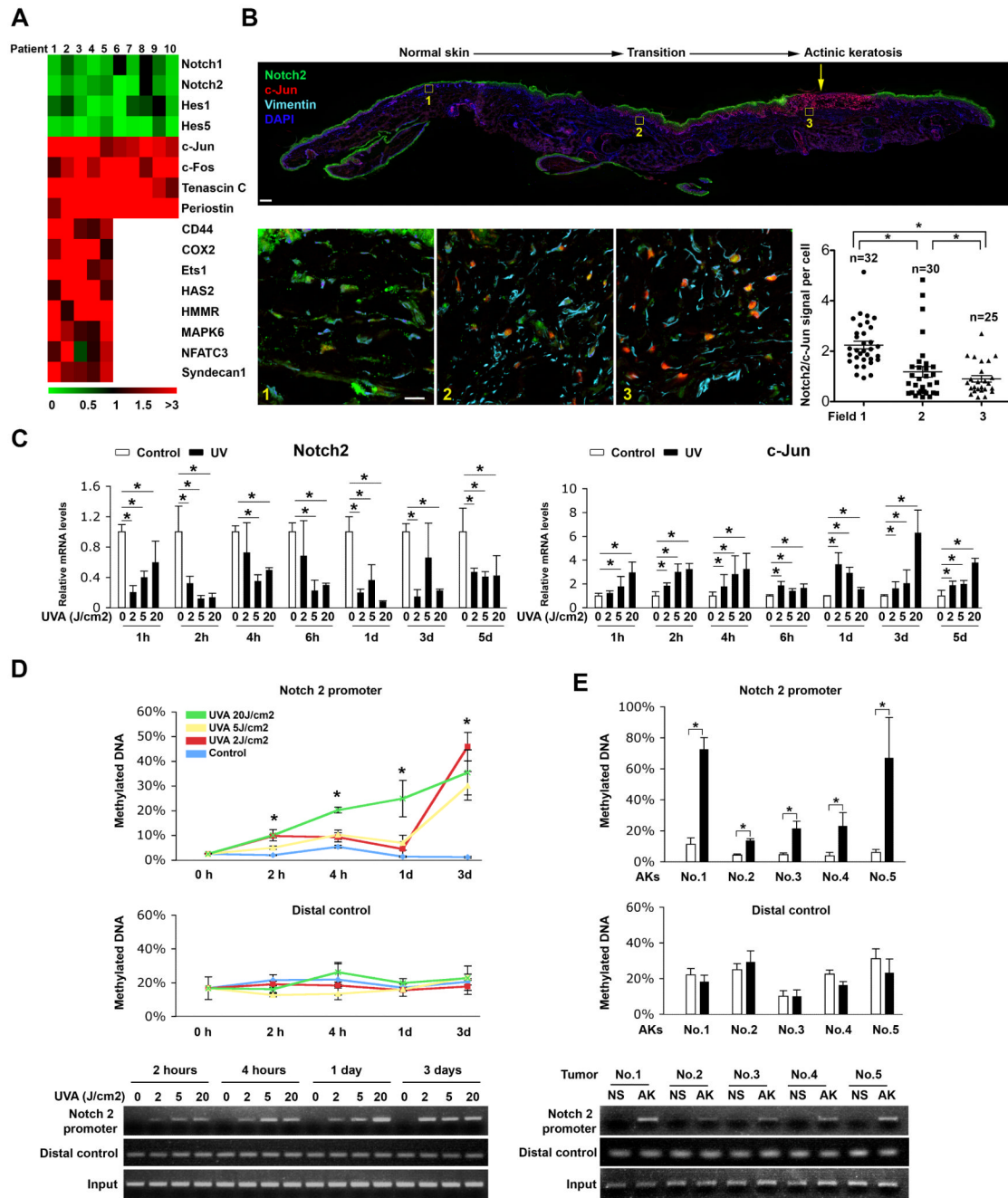
Scale bars: 100μm.

Figure 7. Down-regulation of Notch signaling in stromal fields adjacent to keratinocyte premalignant lesions and impact of UVA exposure

(A) Excised skin samples from 10 patients, containing, in each case, a field of normal epidermis well separated from one with actinic keratosis (AK) lesions were utilized for LCM of the AK underlying stroma versus stroma fields further away, followed by qRT-PCR analysis of indicated genes, using *36β4* for normalization. Results are expressed as heat map of fold changes of the indicated genes in AK-underlying stroma versus stroma further away. Expression of a less complete set of genes could be assessed in part of the cases (from patients #6-10), because of limited sample availability. Effectiveness of the LCM procedure was evaluated by histological analysis of each skin sample before and after stromal removal.

Only upper stromal regions immediately adjacent to the epithelium were captured, which, even in the AK underlying regions, were relatively free of leukocytes (localized instead to the deeper regions). The possibility that leukocyte contamination contributes to observed differences in gene expression was further ruled out by qRT-PCR analysis, showing that *Notch1* and *2* expression was, if anything, higher in purified leukocyte than fibroblast populations, with the reverse being observed for other genes like *c-Jun* (data not shown).

(B) Triple immunofluorescence analysis with antibodies against Notch 2 (green), c-Jun (red) and Vimentin (light blue) of an excised skin sample with an AK lesion. Upper panel: low magnification image illustrating the expected pronounced expression of Notch 2 in upper epidermal layers with Notch2 down-modulation and c-Jun up-regulation in the AK lesion (yellow arrow). Lower panels: higher magnification images for assessment of Notch 2 (green) and c-Jun (red) expression in Vimentin positive (blue) dermal fibroblasts of stromal fields underlying normal epidermis, a transition zone and AK lesion as indicated (fields 1, 2 and 3, respectively). The Notch2 fluorescent signal masked the Vimentin signal and single channel image analysis was used for quantification of Notch2 versus c-Jun signal intensity in Vimentin positive cells (right panel). For this, acquisition of digital images was followed by computer-assisted determination of fluorescence intensity on an individual cell basis. Dots refer to individual measurement values (*$p<0.01$). Scale bars: 200μm, (upper panel); 20μm (lower panels). Analysis of additional AK-containing skin excisions is shown in Fig. S7A-C.

(C) Freshly excised human skin samples placed in semi-solid culture medium and treated with indicated doses of UVA (J/cm2) were withdrawn at indicated times thereafter (hours, days). LCM of upper dermal region followed by qRT-PCR was used to assess expression of indicated genes (*$p<0.01$). Similar results were obtained in other independent experiments with human skin explants and with experiments with cultured human dermal fibroblasts (Fig. S7D-G and data not shown).

(D) Human skin explants exposed to indicated UVA doses were processed at various times thereafter for LCM of the upper dermal region, followed by isolation of CpG-methylated DNA by a binding protein capture method. Methylation levels of the *Notch2* proximal promoter region (161 ntd position rel. to the *Notch2* start site) in untreated versus UVA-treated samples were assessed by qPCR, utilizing total input DNA for normalization. Similar analysis of a distal GC-rich region of the *Notch2* gene (172,856 ntd position rel. to the *Notch2* start site) was performed as equal loading control of partially methylated DNA that is not subject to UVA-induced modulation. Similar analysis of UVA-exposed dermal fibroblasts is shown in (Fig. S7H).

(E) Same skin samples of the first five patients analyzed in (A) were utilized for LCM of AK-underlying versus distal stromal (normal skin, NS) fields, followed by isolation of CpG-methylated DNA as in the previous panel. qPCR analysis was used to assess methylation levels of the *Notch2* promoter and distal GC-rich region (*$p<0.01$).

Scale bars: 200μm, (upper panel of B); 20μm (lower four panels of B).